

# Structure and Properties of $\text{Ag}_2\text{S}/\text{Ag}$ Semiconductor/Metal Hetero-Nanostructure

Sadovnikov, S.I.\*, Gusev, A.I.

Institute of Solid State Chemistry, Ural Branch of the Russian Academy of Sciences, Ekaterinburg-620990, Russia

\***Corresponding author:** Sadovnikov, S.I., a senior research worker of the Laboratory of nonstoichiometric compounds, Institute of Solid State Chemistry, Ural Branch of the Russian Academy of Sciences, Ekaterinburg-620990, Russia, Tel: +7(343)3623034; E-mail: [sadovnikov@ihim.uran.ru](mailto:sadovnikov@ihim.uran.ru)

## Abstract

$\text{Ag}_2\text{S}/\text{Ag}$  hetero-nanostructure has been produced by a simple one-stage chemical deposition from aqueous solutions of silver nitrate, sodium sulfide, and sodium citrate with the use of monochromatic light irradiation. For simultaneous synthesis of  $\text{Ag}_2\text{S}$  and Ag nanoparticles, deposition has been performed from reaction mixtures with reduced sodium sulfide concentration. The formation of  $\text{Ag}_2\text{S}/\text{Ag}$  nanocomposite structures is confirmed by X-ray analysis, high-resolution electron microscopy, energy dispersion analysis and dynamic light scattering methods. It is established that in the contact layer between silver sulfide and silver, non conducting  $\alpha\text{-Ag}_2\text{S}$  acanthite transforms into superionic  $\beta\text{-Ag}_2\text{S}$  argentite under the action of external electric field. The scheme of the operation of a resistive switch based on an  $\text{Ag}_2\text{S}/\text{Ag}$  hetero-nanostructure is proposed.

**Keywords:** Silver sulfide; Silver hetero-nanostructure; Acanthite-argentite phase transformation; Resistive switch

**Received date:** September 12, 2016

**Accepted date:** September 22, 2016

**Published date:** October 27, 2016

**Citation:** Sadovnikov, S.I., et al. Structure and Properties of  $\text{Ag}_2\text{S}/\text{Ag}$  Semiconductor/Metal Hetero-Nanostructure. (2016) J Nanotech Mater Sci 3(2): 27- 36.

**DOI:** 10.15436/2377-1372.16.1114



## Introduction

One of the most requisite semiconducting sulfides is the well known silver sulfide  $\text{Ag}_2\text{S}$ . As early as in 1833, Faraday found that lead fluoride and silver sulfide possessed high ion conductivity comparable to the conductivity of metals in a wide temperature range<sup>[1]</sup>. He wrote: "I formerly described a substance, sulfuret of silver, whose conducting power was increased by heat... When a piece of that substance, which had been fused and cooled, was introduced into the circuit of a voltaic battery, it stopped the current. Being heated, it acquired conducting powers..."<sup>[2]</sup>.

Unique chemical, structural, optical and conductive properties make silver sulfide an excellent substance for preparation of hetero-structures.

Among composite hetero-structures of silver sulfide, the semiconductor/metal hetero-nanostructure  $\text{Ag}_2\text{S}/\text{Ag}$  attracts special attention. It can be used in resistive switches and nonvolatile memory devices<sup>[3-6]</sup>. The action of the switch is based on the phase transformation between nonconducting  $\alpha\text{-Ag}_2\text{S}$  acanthite and superionic  $\beta\text{-Ag}_2\text{S}$  argentite. According to the phase diagram of the system  $\text{Ag} - \text{S}$ <sup>[7]</sup>, silver sulfide  $\text{Ag}_2\text{S}$  has three basic polymorphic modifications]. Low-temperature semiconducting phase  $\alpha\text{-Ag}_2\text{S}$  (acanthite) with monoclinic crystal structure exists at temperatures below  $\sim 450$  K. Monoclinic acanthite has a direct band gap of 0.9-1.05 eV. Under equilibrium conditions, cubic phase  $\beta\text{-Ag}_2\text{S}$  (argentite) exists in the temperature range 452–859 K and has a superionic conductivity. High-temperature Face Centered Cubic (FCC) phase  $\gamma\text{-Ag}_2\text{S}$  stable from  $\sim 860$  K up to melting temperature.

Known methods for the preparation of a hetero-nanostructures of  $\text{Ag}_2\text{S}$  or Ag mainly deal with the synthesis of nanoparticles of one species with the subsequent growth of other species nanoparticles<sup>[8-12]</sup>. These methods are rather expensive and time-consuming.



Chemical deposition is a promising route for preparing nanostructured semiconducting nanoparticles<sup>[13-17]</sup>, thin-film structures and hetero-nanostructures<sup>[9,18]</sup>. By varying the concentration of reagents it is possible to change the number of sulfide phase nuclei in the initial moment of deposition and their growth rate. Thanks to this and different duration of deposition, sulfide particles with controllable size can be obtained. However the preparation of sulfide nanostructures from colloidal solutions is studied insufficiently and the conditions of synthesis as a rule are determined empirically.

Present paper is devoted to study of synthesis conditions of Ag<sub>2</sub>S/Ag hetero-nanostructures by hydrochemical deposition method and determination of their structural characteristics. Present work is a continuation of a cycle of systematic studies of nanostructured silver sulfide<sup>[16,17,19-23]</sup> beginning with synthesis conditions, crystal structure, size and morphology of nanoparticles and ending with phase transformations and thermal properties of nanostructured Ag<sub>2</sub>S.

## Experimental

Ag<sub>2</sub>S/Ag hetero-nanostructures have been synthesized by chemical deposition from aqueous solutions of AgNO<sub>3</sub>, Na<sub>2</sub>S, and Na<sub>3</sub>C<sub>6</sub>H<sub>5</sub>O<sub>7</sub> ≡ Na<sub>3</sub>C it under light irradiation with reduced (as compared with expected silver sulfide stoichiometry) concentration of sodium sulfide (Table 1). Earlier nanocrystalline Ag<sub>2</sub>S sulfide has been synthesized by the same method but without photo irradiation<sup>[19]</sup>. For comparison, Ag<sub>2</sub>S nanoparticles without an impurity of metallic Ag have been synthesized in the dark from reaction mixture with small excess of Na<sub>2</sub>S, i.e.,

$$C_{\text{Na}_2\text{S}} = (C_{\text{AgNO}_3} / 2) + \delta$$

where  $\delta = 0.5 \text{ mmol}\cdot\text{l}^{-1}$  (Table 1).

**Table 1:** Composition of the reaction mixtures, average particle size  $D_{\text{aver}}$  and content of Silver sulfide Ag<sub>2</sub>S and Ag in the Ag<sub>2</sub>S/Ag hetero-nanostructures.

No.	Concentration of reagents in the reaction mixture (mmol·l <sup>-1</sup> )			D <sub>aver</sub> (nm) in deposited powders		D <sub>aver</sub> (nm) in colloidal solutions				Content of Ag <sub>2</sub> S and Ag in Ag <sub>2</sub> S/Ag hetero-nanostructures			
	AgNO <sub>3</sub>	Na <sub>2</sub> S	Na <sub>3</sub> Cit	BET <sup>2)</sup>	XRD <sup>3)</sup>	Ag <sub>2</sub> S		Ag		Ag <sub>2</sub> S		Ag	
						DLS	TEM	DLS	TEM	C <sup>4)</sup> (wt.%)	N <sup>5)</sup> (%)	C <sup>4)</sup> (wt.%)	N <sup>5)</sup> (%)
1	50	25 - δ <sup>1)</sup>	100	56	48 ± 6	28 ± 6	36	9 ± 2	12	95.0	68	5.0	32
2	50	25 - δ <sup>1)</sup>	25	84	52 ± 8	32 ± 6	38	14 ± 3	15	92.5	61	7.5	39
3	50	25 - δ <sup>1)</sup>	12.5	56	46 ± 6	34 ± 6	42	11 ± 3	16	98.0	56	2.0	44
4	50	25 + δ <sup>1)</sup>	10	-	55 ± 6	18 ± 5	35	-	-	100.0	100.0	0	0

<sup>1)</sup>  $\delta = 0.5 \text{ mmol}\cdot\text{l}^{-1}$  (small deficiency of Na<sub>2</sub>S is necessary for the synthesis of Ag<sub>2</sub>S/Ag hetero-nanostructures, small excess of Na<sub>2</sub>S is necessary for synthesis of Ag<sub>2</sub>S nanoparticles without an impurity of metallic Ag);

<sup>2)</sup> Average size  $D_{\text{aver}}$  of Ag<sub>2</sub>S/Ag nanocomposite particles;

<sup>3)</sup> Average size  $D_{\text{aver}}$  of Ag<sub>2</sub>S nanoparticles;

<sup>4)</sup> C is weight content of Ag<sub>2</sub>S and Ag;

<sup>5)</sup> N is relative number of Ag<sub>2</sub>S and Ag nanoparticles.

All the Ag<sub>2</sub>S/Ag hetero-nanostructures were examined by XRD method on a Shimadzu XRD-7000 and STADI-P (STOE) diffractometers in CuK $\alpha_1$  radiation. The XRD measurements were performed in the angle interval  $2\theta = 20 - 95^\circ$  with a step of  $\Delta(2\theta) = 0.02^\circ$  and scanning time of 10 sec in each point. The determination of the crystal lattice parameters and final refinement of the structure of synthesized hetero-nanostructures were carried out with the use of the X'Pert High Score Plus software package<sup>[24]</sup>.

The average particle size D (to be more precise, the average size of Coherent Scattering Regions (CSR)) in deposited silver sulfide powders was estimated by XRD method from the diffraction reflection broadening using the dependence of reduced reflection broadening  $\beta^*(2\theta) = [\beta(2\theta)\cos\theta] / \lambda$  on the scattering vector  $s = (2\sin\theta) / \lambda$ <sup>[15,25]</sup>. The value of broadening  $\beta(2\theta)$  was determined by comparing the experimental width of each diffraction reflection,  $\text{FWHM}_{\text{exp}}$ , with the instrumental resolution function  $\text{FWHM}_R$  of the X-ray diffractometer as  $\beta(2\theta) = [(\text{FWHM}_{\text{exp}})^2 - (\text{FWHM}_R)^2]^{1/2}$ . The resolution function  $\text{FWHM}_R(2\theta) = (u\tan^2\theta + v\tan\theta + w)^{1/2}$  of the Shimadzu XRD-7000 diffractometer was determined in a special diffraction experiment using the cubic lanthanum hexaboride LaB<sub>6</sub> (NIST Standart Reference Powder 660a) with lattice constant  $a = 0.41569162 \text{ nm}$ . The parameters of this resolution function  $\text{FWHM}_R(2\theta)$  are  $u = 0.00616$ ,  $v = -0.00457$ , and  $w = 0.00778$ .

The Ag<sub>2</sub>S/Ag hetero-nanostructures were examined by high-resolution transmission electron microscopy (HRTEM) method also. The HRTEM images were recorded on a JEOL JEM-2010 transmission electron microscope with 140 pm (1.4 Å) lattice resolution. The elemental chemical composition of all the types of nanostructured silver sulfide was studied on the same microscope with the use of an Phoenix (EDAX) Energy Dispersive Spectrometer with a Si(Li) detector having energy resolution of 130 eV. For examination, colloidal solutions of Ag<sub>2</sub>S nanoparticles were placed on a copper grid with collodium-glue covering. One or two layers of collodium-glue (alcoholic solution of kolloksilin) were applied to Cu grid. After the drying of the glue coating, a carbon-containing grid with voids is formed.

The microstructure, size and elemental chemical composition of Ag<sub>2</sub>S/Ag hetero-nanostructures were studied by the Scanning Electron Microscopy (SEM) method on a JEOL-JSM LA 6390 microscope coupled with a JED 2300 Energy Dispersive X-ray Analyzer.

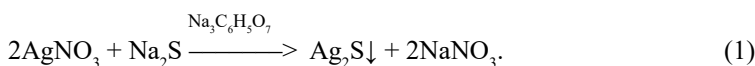
The average particle size  $D$  was also estimated from the value of specific surface area  $S_{sp}$ . The specific surface area  $S_{sp}$  of the synthesized silver sulfide powders was found by the Brunauer-Emmett-Teller (BET) method from the isotherms of low-temperature adsorption of molecular nitrogen vapors at 77 K. The measurements were carried out by means of a Gemini VII 2390t Surface Area Analyzer. In the approximation that all particles have similar size and spherical shape, the average particle size  $D$  is equal to  $6/\rho S_{sp}$  ( $\rho = 7.25 \text{ g}\cdot\text{cm}^{-3}$  is the density of silver sulfide).

The size (hydrodynamic diameter)  $D_{dls}$  of the nanoparticles in the colloidal solutions was determined by non-invasive Dynamic Light Scattering (DLS) on a Zetasizer Nano ZS facility (Malvern Instruments Ltd) at 298 K. The He-Ne laser wavelength was 633 nm, the detection angle of back-scattering light was  $173^\circ$ . To provide reproducibility of the results, light scattering and particle size in each solution were measured minimum 3 times. Treatment of measurement results of particle size distribution was performed using multiple narrow modes with high resolution.

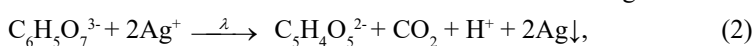
## Results and Discussion

In the reaction mixtures with reduced concentration of  $\text{Na}_2\text{S}$ , along with the formation of  $\text{Ag}_2\text{S}$  sulfide, silver Ag nanoparticles are deposited. Controlling the synthesis conditions,  $\text{Ag}_2\text{S}/\text{Ag}$  hetero-nanostructures can be produced with different ratio of Ag and  $\text{Ag}_2\text{S}$  nanoparticle sizes.

Synthesis was carried out in the following sequence: a complexing agent was added to silver nitrate in the dark; then a solution of  $\text{Na}_2\text{S}$  was poured into the prepared solution (Figure 1(a)). As a result, deposition of silver sulfide occurred by the following reaction :



Further the solution was irradiated with monochromatic light with wavelength 450 nm. In accordance with photochemical reaction,



the citrate ions  $\text{C}_6\text{H}_5\text{O}_7^{3-}$  reduce the  $\text{Ag}^+$  ions to Ag nanoparticles in aqueous solutions and transform into acetone-1,3-dicarboxylate ions  $\text{C}_5\text{H}_4\text{O}_5^{2-}$ . The reduction of silver at the surface of  $\text{Ag}_2\text{S}$  nanoparticles leads to the formation of the  $\text{Ag}_2\text{S}/\text{Ag}$  hetero-nanostructures.

Sodium citrate plays a triple role in synthesis of  $\text{Ag}_2\text{S}/\text{Ag}$  hetero-nanostructures. Firstly, it is a complexing and stabilizing agent during deposition of  $\text{Ag}_2\text{S}$  sulfide nanoparticles. Secondly, during deposition in the light sodium citrate reduce the  $\text{Ag}^+$  ions to metallic silver nanoparticles. Thirdly, citrate is absorbed on nanoparticles and prevents their agglomeration. TEM and HRTEM images of  $\text{Ag}_2\text{S}$ , Ag and  $\text{Ag}_2\text{S}/\text{Ag}$  particles and their diffraction patterns are shown in (Figure 1).

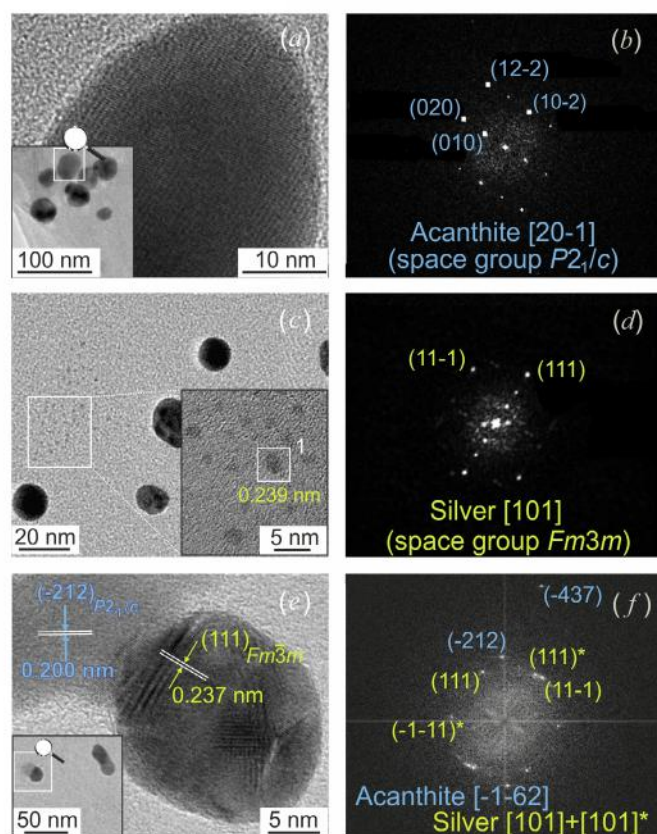


**Figure 1:** TEM and HRTEM images of (a)  $\text{Ag}_2\text{S}$  nanoparticles, (c) Ag nanoparticles, and (e)  $\text{Ag}_2\text{S}/\text{Ag}$  hetero-nanostructures, and FFT patterns (b), (d), and (f) obtained from the (a), (c), and (e) HRTEM images, respectively.

The diffraction patterns (Figure 1(b), 1(d), and 1(f)) of these particles are obtained by Fast Fourier Transformation (FFT) of their HRTEM images. The observed set (Figure 1(b)) of diffraction reflections and interplanar distances of silver sulfide nanoparticle corresponds to monoclinic (space group  $P2_1/c$ ) nanocrystalline acanthite  $\alpha\text{-Ag}_{1.93}\text{S}^{[19]}$ . The Ag nanoparticle with cubic (space group  $Fm\bar{3}m$ ) structure clearly exhibits microtwinning in the direction of the  $[111]$  planes. The performed FFT of the HRTEM image of silver nanoparticle confirms the observed twinning (Figure 1(d)). Diffraction (Figure (f)) obtained by FFT of HRTEM image (Figure 1(e)) of  $\text{Ag}_2\text{S}/\text{Ag}$  hetero-nanostructure revealed reflections of monoclinic silver sulfide and twinned reflections of cubic silver.

According to the EDX results, the content of silver Ag and sulfur S in  $\text{Ag}_2\text{S}$  nanoparticle is equal  $\sim 86.3 \pm 0.4$  and  $\sim 12.9 \pm 0.1$  wt.% and corresponds to  $\sim \text{Ag}_{1.95-1.98}\text{S}$  sulfide. Ag nanoparticle contains silver only, and  $\text{Ag}_2\text{S}/\text{Ag}$  hetero-nanostructure which is shown in (Figure 1(e)) contains about 87.8 and 11.5 wt. % of Ag and S, respectively.

The XRD pattern of  $\text{Ag}_2\text{S}/\text{Ag}$  hetero-nanostructure produced from reaction mixture 2 is shown in Figure 2a. The hetero-nanostructure contains two phases – monoclinic silver sulfide with  $\alpha\text{-Ag}_2\text{S}$  acanthite structure and metallic cubic silver Ag. Detailed XRD studies of the crystal structure of  $\alpha\text{-Ag}_2\text{S}$  acanthite and  $\beta\text{-Ag}_2\text{S}$  argentite phases were performed earlier in our works<sup>[16,19,21,22]</sup>. The quantitative analysis of the XRD pattern (Figure 2a) and comparison with data<sup>[19]</sup> have shown that the observed set of diffraction reflections corresponds to nanocrystalline nonstoichiometric monoclinic (space group  $P2_1/c$ ) acanthite  $\alpha\text{-Ag}_{1.93}\text{S}$  and cubic (space group  $Fm\bar{3}m$ ) silver Ag. The Crystallographic Information File (CIF) for cubic (space group  $Im\bar{3}m$ ) argentite  $\beta\text{-Ag}_2\text{S}$  (CCDC reference number 1062400) is presented in our study<sup>[21]</sup> as Electronic Supplementary Information (see DOI: [10.1039/c5cp02499d](https://doi.org/10.1039/c5cp02499d)). The diffraction reflection broadening (see Figure 2a) is indicative of the nanosized state of the both phases. The content of Ag and  $\text{Ag}_2\text{S}$  in the nanopowders deposited from reaction mixtures 1, 2, and 3 is equal to  $\sim 5.0$  and  $\sim 95.0$  wt.%,  $\sim 7.5$  and  $\sim 92.5$ , and  $\sim 2.0$  and  $\sim 98.0$ , respectively (see Table 1).

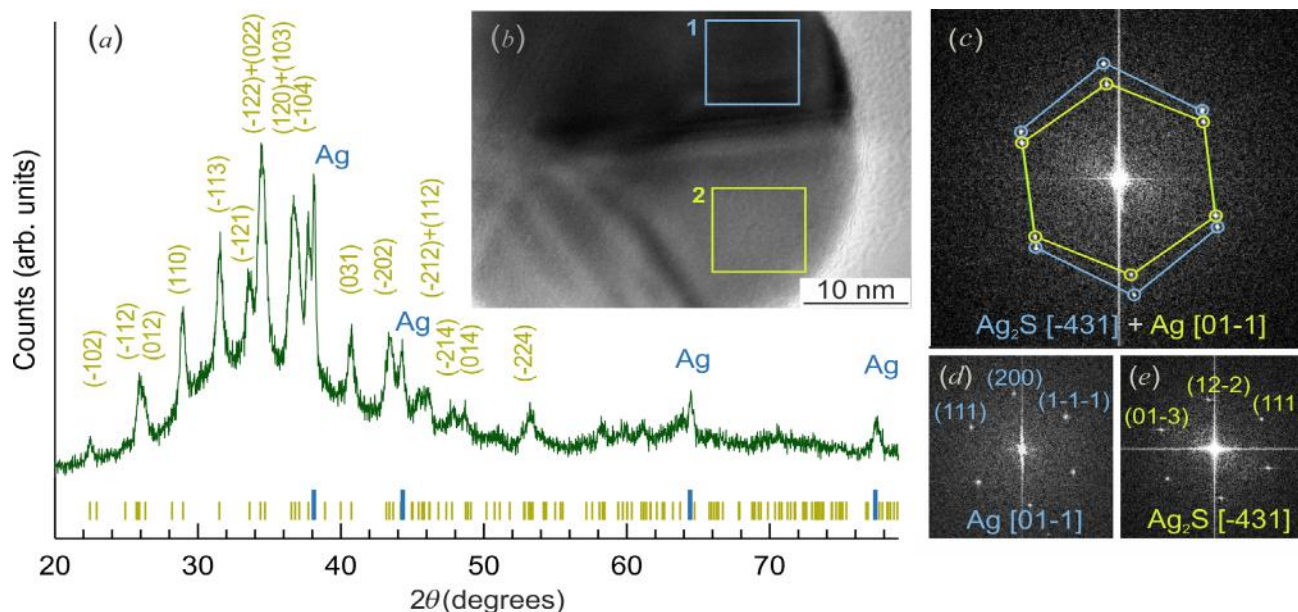


**Figure 2:** (a) XRD pattern and (b) HRTEM image of  $\text{Ag}_2\text{S}/\text{Ag}$  hetero-nanostructure. (c), (d), and (e) diffraction patterns obtained by FFT of HRTEM image of the whole composite hetero-nanostructure and its areas (1) and (2). The long and short ticks on XRD pattern correspond to reflections of cubic metallic Ag and monoclinic  $\text{Ag}_2\text{S}$  silver sulfide, respectively.

For the electron microscopy study of the two-phase nanoparticles, we used the colloidal solutions above the deposited powders. The HRTEM image of  $\text{Ag}_2\text{S}/\text{Ag}$  hetero-nanostructure is shown in Figure 2b. It is seen that the  $\text{Ag}_2\text{S}$  and Ag nanoparticles are in direct contact and form the hetero-nanostructure.

Crystal structure and inter planar distances were determined for single  $\text{Ag}_2\text{S}$  nanoparticles by HRTEM method. Selected Area of Electron Diffraction (SAED) was obtained by standard FFT of selected area of HRTEM image. Then we carried out inverse FFT of the selected diffraction reflections in the HRTEM image using the Gatan Microscopy Suite software<sup>[26]</sup>, and determined the interplanar distances corresponding to these diffraction reflections. The scheme of sequence of operation for determination of the interplanar distances for the diffraction reflections, observed on SAED, is shown in Figure 3.

Detailed description of determination of interplanar distances with the use of the Gatan Microscopy software<sup>[26]</sup> is given on site<sup>[27]</sup>.

In the examination of hetero-nanostructures, it is necessary to determine the crystallographic indices of reflections obtained experimentally by electron diffraction method or FFT of the HRTEM images. This is especially important for exact identification of phase components which form a hetero-nanostructure. For compounds with oblique-angled (triclinic and monoclinic) unit cells, errors are sometimes committed during reflection indexing. In particular, Xu et al.<sup>[4]</sup> incorrectly determined the diffraction reflection indices of monoclinic acanthite  $\alpha\text{-Ag}_2\text{S}$  in  $\text{Ag}/\text{Ag}_2\text{S}/\text{W}$  hetero-nanostructure. Authors<sup>[28]</sup> incorrectly determined the indices of diffraction reflections and interplanar distances of metallic silver for  $\text{Ag}/\text{polypyrrole}$  composite on Si substrate. Such errors can be found in many studies devoted to the  $\text{Ag}_2\text{S}/\text{Ag}$  hetero-nanostructures in which monoclinic (space group  $P2_1/c$ )  $\alpha\text{-Ag}_2\text{S}$  acanthite, cubic

(space group  $Im\bar{3}m$ )  $\beta$ - $Ag_2S$  argentite with Body Centered Cubic (BCC) crystal lattice, and cubic (space group  $Fm\bar{3}m$ ) silver Ag can coexist.

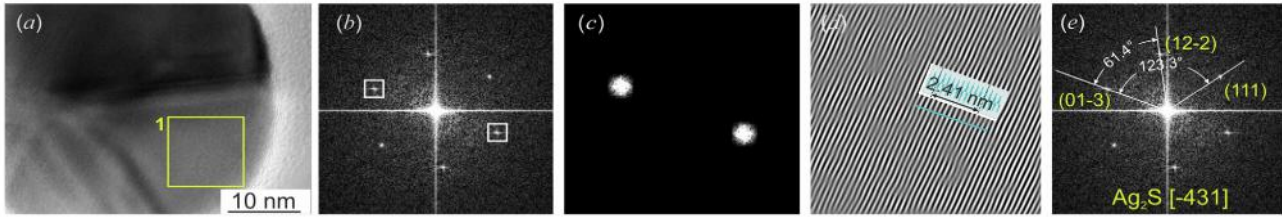


**Figure 3:** Sequence of operation for determination of the interplanar distances includes following steps: (a) uploading of HRTEM image in Gatan Microscopy Suite and selection of area in HRTEM image for FFT (green square); (b) creation of FFT from the selected area and selection of a spot on FFT; (c) creation of a mask from FFT; (d) creation of inverse FFT using mask, creation of line scale profile on FFT, and calculation of interplanar distance; (e) determination of  $(hkl)$  indices. Then steps b, c, d, and e are repeated for another spots.

Usually, the electron diffraction indices  $(hkl)$  are determined by comparing the derived interplanar distances  $d_{hkl}$  with the  $d_{hkl}$  values corresponding to a unit cell with known parameters. The authors<sup>[4]</sup> compared their data on acanthite with stale data<sup>[29]</sup>, according to which the unit cell of monoclinic (space group  $P2_1/n$ ) acanthite  $\alpha$ - $Ag_2S$  has parameters  $a = 0.423$  nm,  $b = 0.691$  nm,  $c = 0.787$  nm and  $\beta = 99.6^\circ$ .

However in low-symmetry structures, the neighbor values of  $d_{hkl}$  differ very slightly forming an almost continuous spectrum. That is why the error in determining the indices  $(hkl)$  of reflections from the value of  $d_{hkl}$  in low-symmetry structures is large. Much more accurately we can determine the angle  $\varphi_{\text{ref}}$  between the reflections with assumed indices  $(h_k l_i)$  on the FFT pattern, i. e. the angle between the straight lines passing through each reflection and the central spot (000). To refine the derived indices, it is necessary to calculate the angles  $\varphi_{\text{ref}}$  between reflections with indices  $(h_k l_i)$  and compare them with the experimental angles between these reflections. The coincidence of the estimated and experimental  $\varphi_{\text{ref}}$  angles unequivocally proves that the indices  $(h_k l_i)$  are determined correctly.

In order to calculate the angles  $\varphi_{\text{ref}}$ , i. e. the angles between the atomic surface normal, it is necessary to transform the non-orthogonal (triclinic or monoclinic) coordinates into rectangular coordinates and then, using the transformed coordinates, to determine the basis vector of the reciprocal cell. For example, the basis vectors  $(100)_{\text{mon}}$ ,  $(010)_{\text{mon}}$  and  $(001)_{\text{mon}}$  of the monoclinic unit cell written in rectangular coordinates have the form  $\mathbf{a} = (a00)$ ,  $\mathbf{b} = (0b0)$  and  $\mathbf{c} = (c \cos \beta \ 0 \ c \sin \beta)$ , respectively. The basis vectors of the reciprocal lattice found by the known formula have the form  $\mathbf{a}^* = (1/a \ 0 \ -\cos \beta / (a \sin \beta))$ ,  $\mathbf{b}^* = (0 \ -1/b \ 0)$  and  $\mathbf{c}^* = (0 \ 0 \ 1/(c \sin \beta))$ . Accordingly, the arbitrary vector  $(hkl)_{\text{mon}}^*$  of the reciprocal lattice in the rectangular coordinate system has the explicit form

$$(hkl)_{\text{mon}}^* = h\mathbf{a}^* + k\mathbf{b}^* + l\mathbf{c}^* \equiv \left( \frac{h}{a} \quad -\frac{k}{b} \quad \frac{al - hc \cos \beta}{ac \sin \beta} \right) \quad (3)$$

where  $h_{\text{cub}} = h/a$ ,  $k_{\text{cub}} = -k/b$  and  $l_{\text{cub}} = (al - hc \cos \beta) / (ac \sin \beta)$ .

The angle  $\varphi_{\text{ref}}$  between reflections  $(h_1 k_1 l_1)$  and  $(h_2 k_2 l_2)$  in the rectangular coordinate system is determined by the standard formula

$$\cos \varphi = \frac{h_{1\text{cub}} h_{2\text{cub}} + k_{1\text{cub}} k_{2\text{cub}} + l_{1\text{cub}} l_{2\text{cub}}}{\sqrt{h_{1\text{cub}}^2 + k_{1\text{cub}}^2 + l_{1\text{cub}}^2} \times \sqrt{h_{2\text{cub}}^2 + k_{2\text{cub}}^2 + l_{2\text{cub}}^2}} \quad (4)$$

Replacing in eq. (4) the cubic indices  $h_{\text{cub}}$ ,  $k_{\text{cub}}$  and  $l_{\text{cub}}$  by their values expressed through monoclinic indices  $h$ ,  $k$  and  $l$ , we obtain the formula for determining the angles  $\varphi_{\text{ref}}$  between the reflections  $(h_1 k_1 l_1)_{\text{mon}}$  and  $(h_2 k_2 l_2)_{\text{mon}}$  in the reciprocal lattice of monoclinic structure

$$\cos \varphi = \frac{h_1 h_2 / a^2 + k_1 k_2 / b^2 + [l_1 l_2 a^2 - (h_1 l_2 + h_2 l_1) ac \cos \beta + h_1 h_2 c^2 \cos^2 \beta] / (ac \sin \beta)^2}{d_1 \times d_2} \quad (5)$$

Where  $d_i = \sqrt{(h_i / a)^2 + (k_i / b)^2 + [(l_i a - h_i c \cos \beta) / (ac \sin \beta)]^2}$  with  $i = 1$  or  $2$ .

It is easily seen that expression (5) at  $\beta = 90^\circ$  is transformed into a standard expression suitable for the description of structures with orthogonal (orthorhombic, tetragonal, cubic) unit cells.

As an example, at the top of Figure 4 there is Figure 2 borrowed from article<sup>[4]</sup> with a HRTEM image of monoclinic acan-

thite and an incorrect indexing of reflections on the FFT patterns obtained from regions (1) and (2) of this image. At the bottom of Figure 4, correct indexing of the same reflections with allowance for the experimental values of angles  $\varphi_{\text{refl}}$  is shown.

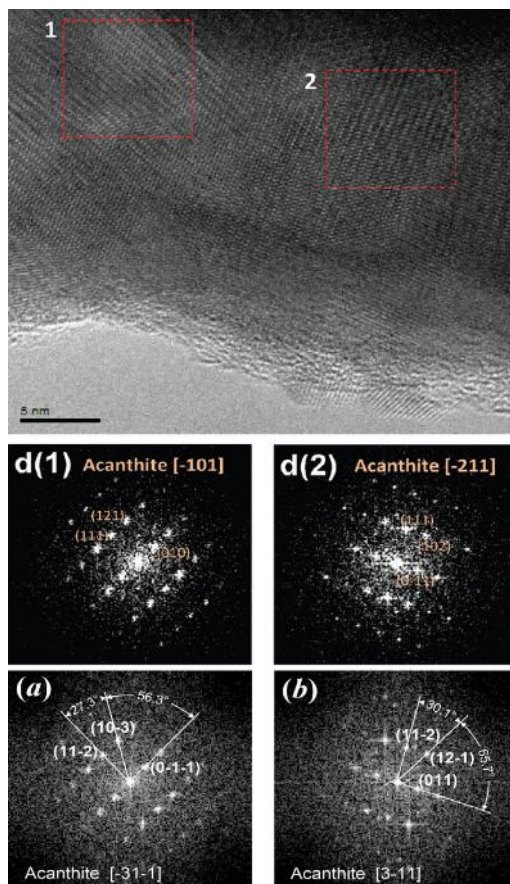


**Figure 4:** The HRTEM image of monoclinic acanthite from article<sup>[4]</sup> and indexing of reflections on the FFT patterns obtained from different regions (1) and (2) of this image. (d1) and (d2) are incorrect reflection indices reported in study<sup>[4]</sup>. (a) and (b) are correct reflection indices on the FFT patterns obtained from regions (1) and (2).

For instance, in Figure 4 d1 the experimental angles between the hypothetical reflections (111) and (121) or between (121) and (010) are equal to  $\sim 27.3^\circ$  and  $\sim 56.3^\circ$ <sup>[4]</sup>. The angles between such reflections, which were estimated in study<sup>[4]</sup>, should be  $17.8^\circ$  and  $45.1^\circ$  and they do not coincide with the experimental values. Consequently, the reflection indices are determined incorrectly. We have determined the indices of these reflections using region 1 on the HRTEM image (Figure 4) in article<sup>[4]</sup>. These reflections have indices (11-2), (10-3) and (0-1-1), the calculated angles between them are equal to  $27.0^\circ$  and  $56.6^\circ$ , which coincides with the experimental values of  $\varphi_{\text{refl}}$  (Figure 4a). The analysis showed that these reflections are observed along the  $[-31-1]$  zone axis rather than along  $[-101]$  as stated by Xu *et al.*<sup>[4]</sup>.

The indices of diffraction reflections of monoclinic acanthite  $\alpha\text{-Ag}_2\text{S}$  on the FFT pattern (Figure 4d2) and other FFT patterns in study<sup>[4]</sup> are also determined incorrectly. In study<sup>[4]</sup>, only the diffraction reflection indices of cubic (space group  $Fm\bar{3}m$ ) silver Ag and cubic (space group  $Im\bar{3}m$ ) argentite  $\beta\text{-Ag}_2\text{S}$  are determined correctly. Note also that for analysis of the transformation of monoclinic acanthite into cubic argentite, the structure of acanthite would be more properly described in the space group  $P2_1/c$  proposed in work<sup>[30]</sup> and refined for artificial coarse-crystalline acanthite in work<sup>[16]</sup> and for nano crystalline acanthite in work<sup>[19]</sup>.

In order to exclude the errors at experimental determination of angles  $\varphi_{\text{refl}}$ , an area of HRTEM image selected for FFT should have the square form.

As an example, square area (a) of HRTEM image of monoclinic acanthite  $\alpha\text{-Ag}_2\text{S}$  and FFT (b) of this image with indexing of observed diffraction spots and the experimental values of angles  $\varphi_{\text{refl}}$  are shown in Figure 5. The interplanar distances are determined by inverse FFT of the selected diffraction spots using the Gatan Microscopy Suite software<sup>[26]</sup>.

The comparison of found inter planar distances 0.229, 0.204, 0.244, and 0.244 nm (see Figure. 5(b)) with data<sup>[19]</sup> shown that the observed diffraction spots can have following crystallographic indices (030), (023), (013), and (0-13) of monoclinic (space group  $P2_1/c$ ) acanthite.

As is seen, the experimental angles  $\varphi_{\text{refl}}$  between the hypothetical reflections (030) and (023) or between (023) and (0-13) are equal to  $\sim 51.4^\circ$  and  $\sim 57.0^\circ$  (Figure 4(b)). The calculated angles  $\varphi_{\text{refl}}$  between these reflections should be  $53.3^\circ$  and  $57.2^\circ$  and they coincide with the experimental angles within the limits of measurement errors. Analogously, the experimental angles  $\varphi_{\text{refl}}$  between the hypothetical reflections (013) and (0-13) or between (0-13) and (0-30) are equal to  $\sim 39.5^\circ$  and  $\sim 72.2^\circ$ . The calculated angles  $\varphi_{\text{refl}}$  between are equal  $40.9^\circ$  and  $69.5^\circ$  and coincide with the experimental angles. The analysis showed that these reflections are observed along the  $[100]$  zone axis of monoclinic (space group  $P2_1/c$ ) acanthite  $\alpha\text{-Ag}_2\text{S}$ .

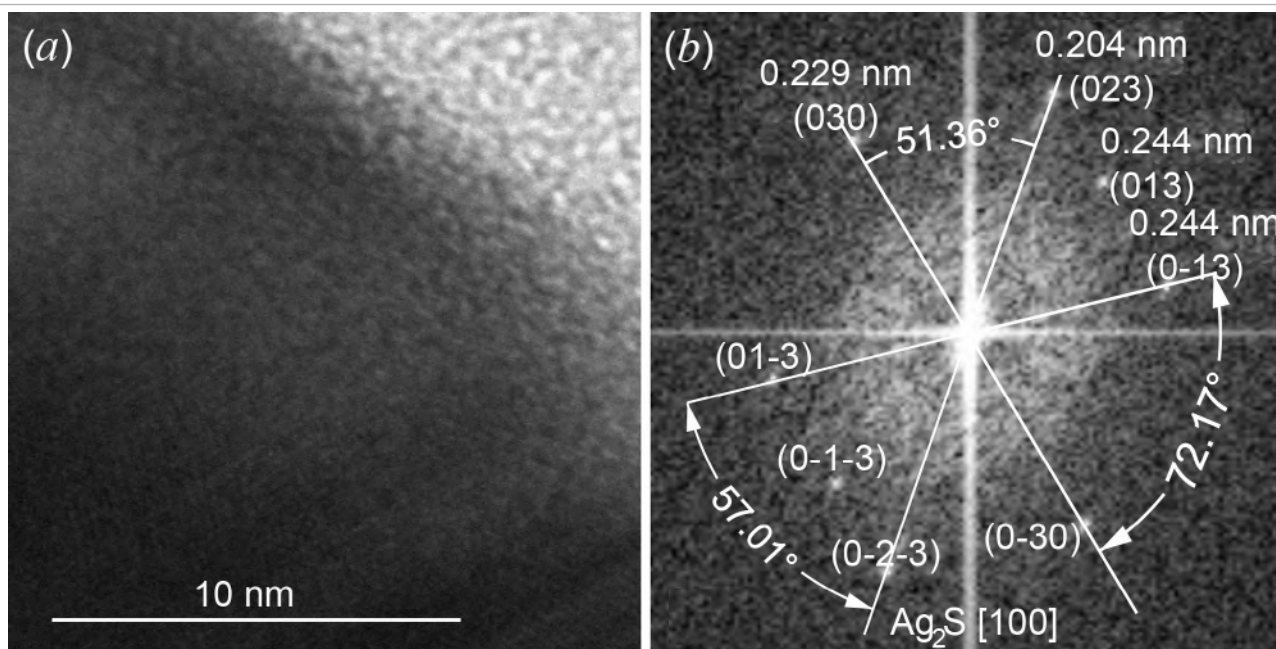


**Figure 5:** The HRTEM image (a) of monoclinic acanthite  $\alpha$ - $\text{Ag}_2\text{S}$  and FFT (b) of this image with indexing of observed diffraction spots and the experimental values of angles  $\varphi_{\text{ref}}$ .

In present study the indices ( $hkl$ ) of the electron diffraction reflections have been determined with taking into account interplanar distances  $d_{hkl}$  and angles  $\varphi_{\text{ref}}$  between observed reflections.

HRTEM image of  $\text{Ag}_2\text{S}/\text{Ag}$  hetero-nanostructure produced from the reaction mixture 2 is shown in Figure 2b. The diffraction pattern (d) obtained by FFT of HRTEM image of the whole this composite hetero-nanostructure contains two set of diffraction reflections corresponding to monoclinic silver sulfide and cubic silver. The diffraction patterns (e) and (f) are obtained by FFT from areas (1) and (2) isolated by green and orange quadrates. The observed set (e) of spots (111), (200), and (1-1-1) corresponds to the [01-1] plane of the reciprocal lattice of cubic Ag. The interplanar distances for area (2) and the set (f) of spots (01-3), (12-2), and (111) correspond to monoclinic  $\alpha$ - $\text{Ag}_2\text{S}$  acanthite.

The DLS measurements of the particle size in colloidal solutions 1, 2, and 3 showed that the size and volume distributions are bimodal (Figure 6). This means that these colloidal solutions contain two groups of particles – small particles and larger particles. Taking into consideration the TEM data for  $\text{Ag}_2\text{S}/\text{Ag}$  hetero-nanostructures, it can be supposed that small particles are Ag particles and larger particles are  $\text{Ag}_2\text{S}$  particles. Thus, the DLS measurements confirm indirectly the presence of Ag and  $\text{Ag}_2\text{S}$  particles in colloidal solutions 1, 2, and 3. The Ag particles are 2 - 3 times smaller in size than the  $\text{Ag}_2\text{S}$  particles. Therefore, the volume of individual Ag particle is  $\sim 10$  - 20 times smaller than the volume of  $\text{Ag}_2\text{S}$  particle. Because of the small volume of Ag particles their amount is comparable with the amount of  $\text{Ag}_2\text{S}$  particles.

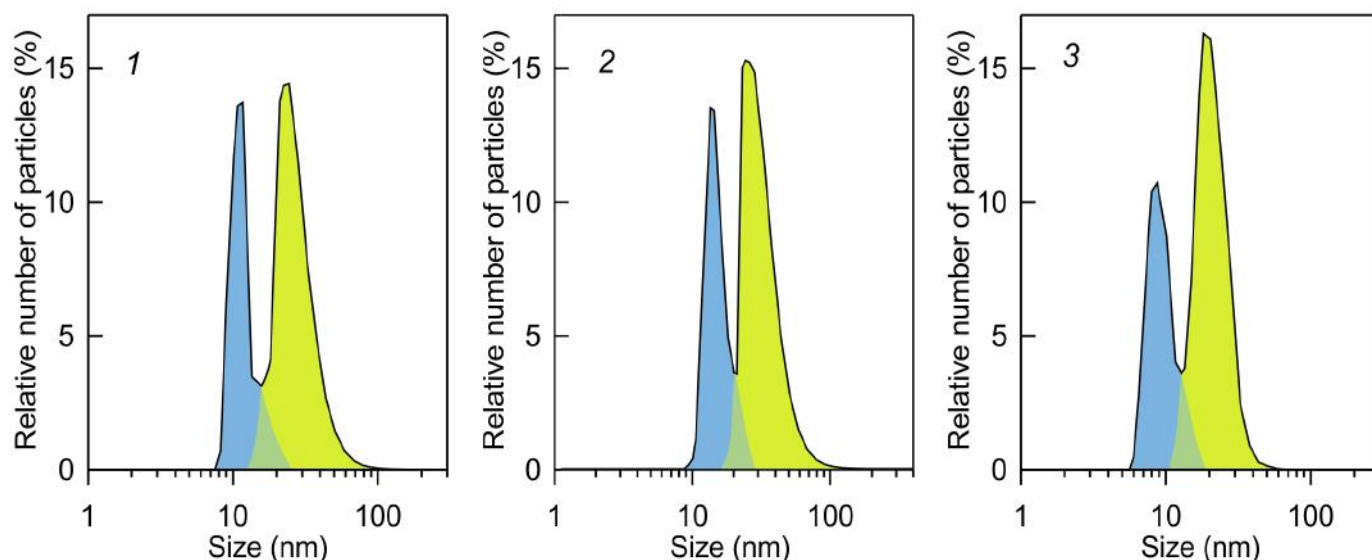


**Figure 6:** Bimodal size distributions of nanoparticles for colloidal solutions 1, 2, and 3. Maxima of distributions at  $\sim 7$ -15 nm correspond to Ag nanoparticles mainly, maxima of distributions in the region of 20 - 50 nm correspond to  $\text{Ag}_2\text{S}$  nanoparticles predominantly.

The produced  $\text{Ag}_2\text{S}/\text{Ag}$  hetero-nanostructures combine ionic and electronic conductors. The heterostructures of this type containing Ag and  $\text{Ag}_2\text{S}$  nano fibers or a silver film with  $\text{Ag}_2\text{S}$  nano clusters are considered as a potential basis for creating biosensors<sup>[31]</sup>, resistive switches and nonvolatile memory devices<sup>[4-6,32]</sup>. The resistive switches consist of a superionic conductor located between two metal electrodes. In the case of  $\text{Ag}_2\text{S}/\text{Ag}$  hetero-structures, one of the electrodes is silver, and the second electrode can be such metals as Pt, Au, and Cu.

In this study,  $\text{Ag}_2\text{S}/\text{Ag}$  hetero-structures formed by  $\text{Ag}_2\text{S}$  and Ag nanoparticles have been produced by a simple method of hydrochemical bath deposition. Deposition of  $\text{Ag}_2\text{S}/\text{Ag}$  hetero-structures on a substrate coated with a thin conducting metallic layer will make it possible to form a structure, which can work as a resistive switch. The action of the switch is based on the phase transformation of nonconducting  $\alpha$ - $\text{Ag}_2\text{S}$  acanthite into  $\beta$ - $\text{Ag}_2\text{S}$  argentite exhibiting superionic conduction. The transition into a high-conduction state is due to abrupt disordering of the cationic sublattice. In studies<sup>[33,34]</sup> it was shown that a high-conduction state of a crystal can be achieved by electric field induced “melting” of the cationic sublattice taking place without heating of the crystal. Such transformation occurring as a result of applied external electric field was confirmed by the authors<sup>[4-6]</sup> with respect to nanocrystalline silver sulfide. The effect of external electric field induced abrupt disordering allows the realization of the superionic state of silver sulfide at room temperature. This opens up the possibilities for practical use of materials based on silver sulfide. Earlier we performed an *in situ* high-temperature scanning electron microscopy study of acanthite - argentite phase transformation during electron beam heating<sup>[21]</sup> and an *in situ* high-temperature XRD study of this transformation<sup>[23]</sup>.

As already noted, the action of the resistive switch is based on the phase transformation of nonconducting  $\alpha$ - $\text{Ag}_2\text{S}$  acanthite into superionic  $\beta$ - $\text{Ag}_2\text{S}$  argentite. This phase transformation in  $\text{Ag}_2\text{S}/\text{Ag}$  hetero-nanostructure can be induced by external electric field without any heating.

We have studied preliminarily the switching processes in  $\text{Ag}_2\text{S}/\text{Ag}$  hetero-nanostructure. For this purpose, a metallic Pt micro contact was supplied to  $\text{Ag}_2\text{S}/\text{Ag}$  hetero-nanostructure and bias voltage was impressed so that Ag electrode was charged positively. When positive bias voltage increases to 500 mV, the conduction of the hetero-nanostructure grows and the nano device transforms into the on-state. The bias back to negative values decreases the conduction and the nano device transforms into the off-state.

Figure 7 displays a region of  $\text{Ag}_2\text{S}/\text{Ag}$  hetero-nanostructure where change of crystal structure at the transition from the off-state (Figure 7(a)) to the on-state (Figure 7(b)) can be observed. Using FFT of HRTEM images, we obtained the diffraction patterns (Figure 7(c), 7(d)).

The diffraction pattern in (Figure 7(c)) contains (111), (11-1) spots and twinning reflection (111)\* corresponding to cubic (space group  $Fm\bar{3}m$ ) silver, as well as (2-12) and (030) spots corresponding to monoclinic (space group  $P2_1/c$ )  $\alpha$ - $\text{Ag}_2\text{S}$  acanthite. The observed angle of  $100.3^\circ$  between (2-12) and (030) spots of monoclinic acanthite coincides within measurement error with the theoretical value  $100.7^\circ$ .

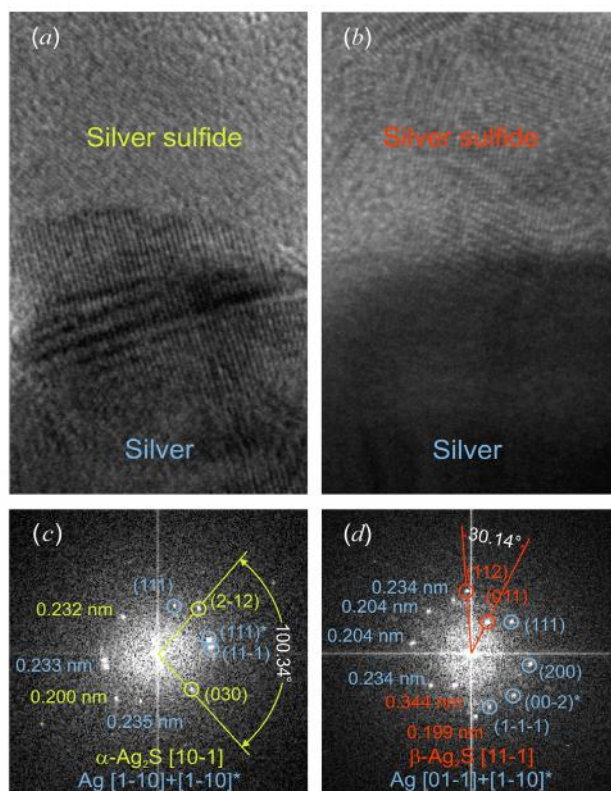


**Figure 7:** HRTEM images of region of transition between Ag and  $\text{Ag}_2\text{S}$  for off-state (a) and on-state (b) of  $\text{Ag}_2\text{S}/\text{Ag}$  hetero-nanostructure. The on-state arises as a result of applied external positive bias voltage to this  $\text{Ag}_2\text{S}/\text{Ag}$  hetero-nanostructure. The Pt electrode is located on the top part of the image, and Ag electrode is in the bottom part. Diffraction patterns (c) and (d) are obtained by FFT of HRTEM images (a) and (b), respectively. When  $\text{Ag}_2\text{S}/\text{Ag}$  hetero-nanostructure is transformed from the off-state into the on-state, along with Ag spots, the (011) and (112) spots of  $\beta$ - $\text{Ag}_2\text{S}$  argentite appear on the diffraction pattern (d) instead of acanthite spots.



The diffraction pattern (Figure 7(d)) contains two sets of spots corresponding to two cubic phases. The (111), (200), (1-1-1) spots and the twinning spot (00-2)\* correspond to cubic (space group  $Fm\bar{3}m$ ) silver, and the (011) and (112) spots correspond to cubic (space group  $Im\bar{3}m$ )  $\beta$ - $\text{Ag}_2\text{S}$  argentite. The observed angle of  $30.1^\circ$  between the (011) and (112) spots of cubic  $\beta$ - $\text{Ag}_2\text{S}$  argentite coincides with the theoretical value  $30^\circ$ . Experimental angles between diffraction spots of cubic silver (Figure 7c, 7d) coincide with theoretical values. Thus, the applied bias really leads to the appearance of conducting  $\beta$ - $\text{Ag}_2\text{S}$  argentite instead of nonconducting  $\alpha$ - $\text{Ag}_2\text{S}$  acanthite.

The operation of a switch based on silver sulfide is schematically illustrated in (Figure 8).

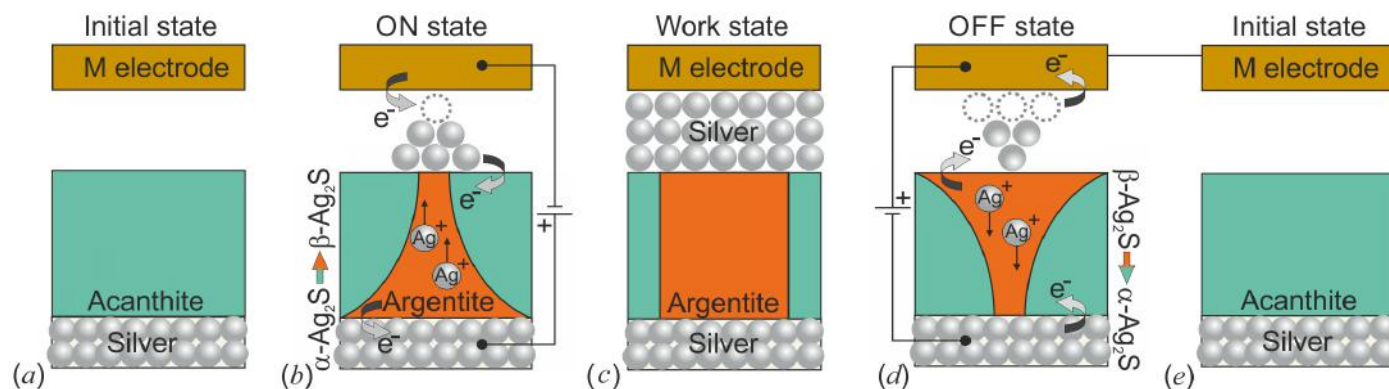


**Figure 8:** Scheme of the operation of an  $\text{Ag}_2\text{S}/\text{Ag}$ -based switch: (a) initial non conducting state, (b) the appearance of a conductive channel upon the application of an external electric field that induces the transformation of acanthite  $\alpha$ - $\text{Ag}_2\text{S}$  into argentite  $\beta$ - $\text{Ag}_2\text{S}$ , (c) a continuous conductive channel, (d) break down of the conductive channel upon the application of negative bias and the transition of argentite into initial acanthite, and (e) the disappearance of the conductive channel and turning-off of the switch.

The initial  $\text{Ag}_2\text{S}$  phase is a nonconducting acanthite  $\alpha$ - $\text{Ag}_2\text{S}$  (Figure 8(a)). When a positive bias is applied,  $\text{Ag}^+$  cations start to move toward the negatively charged cathode M and are reduced to Ag atoms during their transport. At the same time, the  $\alpha$ - $\text{Ag}_2\text{S}$  phase transforms into superionic  $\beta$ - $\text{Ag}_2\text{S}$  argentite (Figure 8(b)), and a continuous conductive channel is formed (Figure 8(c)). The continuous conductive channel which is formed from argentite  $\beta$ - $\text{Ag}_2\text{S}$  and silver Ag is retained, when the external field is turned off. This phenomenon can be considered as a memory effect (Figure 8(c)). If a negative (reverse) bias is applied to the switch, the Ag nanocrystals start dissolving in argentite, the  $\text{Ag}^+$  cations move to the anode, argentite transforms into the initial acanthite again, and the conductive channel breaks down (Figure 8(d)). Because of the formation of nonconducting acanthite, the conductive channel disappears; the switch transforms into the initial state and is turned off (Figure 8(e)). If positive bias is applied once again, the destroyed conductive channel is restored due to the appearance of argentite and the formation of silver. According to<sup>[3,6]</sup>, the bias voltage which is sufficient to turn on and off the switch is in range from  $\pm 0.2$  to  $\pm 10.0$  V depending on the metal M used as the second electrode.

## Conclusion

The  $\text{Ag}_2\text{S}/\text{Ag}$  hetero-nanostructures are formed in aqueous solutions of  $\text{AgNO}_3$ ,  $\text{Na}_2\text{S}$ , and  $\text{Na}_3\text{C}$  it with decreased concentration of sodium sulfide during synthesis in the light. The appearance of Ag nanoparticles is due to photochemical reduction of some  $\text{Ag}^+$  ions by citrate ions.

The produced  $\text{Ag}_2\text{S}/\text{Ag}$  hetero-nanostructures combine ionic and electronic conductors. A high-conducting state of such hetero-nanostructure can be induced by external electric field without heating of this composite owing to phase transformation of nonconducting acanthite into argentite exhibiting superionic conduction. The argentite  $\alpha$ - $\text{Ag}_2\text{S}$  which appears as a result of the phase transformation and metallic silver Ag together form the conducting channel. The scheme of the operation of a resistive switch based on an  $\text{Ag}_2\text{S}/\text{Ag}$  hetero-nanostructure is proposed. The main application of  $\text{Ag}_2\text{S}/\text{Ag}$  hetero-nanostructure is a creation of resistive switches and nonvolatile memory devices.

**Acknowledgement:** This work is financially supported by the Russian Science Foundation (Grant 14-23-00025) through the Institute of Solid State Chemistry of the Ural Branch of the RAS. Authors are grateful to Dr. E.Yu. Gerasimov for the help in some TEM measurements.

**Conflict of Interest:** The authors declare no conflict of interests.

## References

1. Faraday, M. Experimental researches in electricity. - Fourth series. (1833) Philosophical Transactions of the Royal Society of London 123: 507-522.
2. Faraday, M. Experimental researches in electricity. - Twelfth series. (1838) Phil Trans Royal Soc Lond 128: 83-123.
3. Liang, C.H., Terabe, K., Hasegawa, T., et al. Resistance switching of an individual Ag<sub>2</sub>S/Ag nano wire hetero structure. (2007) Nanotechnology 18(48): 485202.
4. Xu, Z., Bando, Y., Wang, W., et al. Real-time in situ HRTEM-resolved resistance switching of Ag<sub>2</sub>S nanoscale ionic conductor. (2010) ACS Nano 4(5): 2515-2522.
5. Wang, D., Liu, L., Kim, Y., et al. Fabrication and characterization of extended arrays of Ag<sub>2</sub>S/Ag nano dot resistive switches. (2011) Appl Phys Lett 98(24): 243109.
6. Belov, A.N., Pyatlova, O.V., Vorobiev, M.I. Synthesis of Ag/Ag<sub>2</sub>S nanoclusters resistive switches for memory cells. (2014) ANP 3(1): 1-4.
7. Sharma, R.C., Chang, Y.A. The Ag-S (silver-sulfur) system. (1986) Bulletin of Alloy Phase Diagrams 7(3): 263-269.
8. Pang, M.L., Hu, J.Y., Zeng, H.C. Synthesis, morphological control, and antibacterial properties of hollow/solid Ag<sub>2</sub>S/Ag heterodimers. (2010) J Am Chem Soc 132(31): 10771-10785.
9. Yang, J., Ying, J.Y. Nanocomposites of Ag<sub>2</sub>S and noble metals. (2011) Angew Chem Int Ed 50(20): 4637-4643.
10. Pacholski, C., Kornowski, A., Weller, H. Site-specific photodeposition of silver on ZnO nanorods. (2004) Angew Chem Int Ed Engl 43(36): 4774-4777.
11. Fan, F.R., Ding, Y., Liu, D., et al. Facet-selective epitaxial growth of heterogeneous nanostructures of semiconductor and metal: ZnO nanorods on Ag nanocrystals. (2009) J Am Chem Soc 131(34): 12036-12037.
12. Yang, J., Ying, J.Y. Room-temperature synthesis of nanocrystalline Ag<sub>2</sub>S and its nanocomposites with gold. (2009) Chem Commun (Camb) 14(22): 3187-3189.
13. Zhang, W., Zhang, L., Hui, Z., et al. Synthesis of nanocrystalline Ag<sub>2</sub>S in aqueous solution. (2000) Solid State Ionics 130(1-2): 111-114.
14. Pawar, S.M., Pawar, B.S., Kim, J.H., et al. Recent status of chemical bath deposited metal chalcogenide and metal oxide thin films. (2011) Current Applied Physics 11(2): 117-161.
15. Sadovnikov, S.I., Gusev, A.I. Chemical deposition of nanocrystalline lead sulfide powders with controllable particle size. (2014) Journal of Alloys and Compounds 586: 105-112.
16. Sadovnikov, S.I., Gusev, A.I., Rempel, A.A. Artificial silver sulfide Ag<sub>2</sub>S: crystal structure and particle size in deposited powders. (2015) Superlattices and Microstructures 83: 35-47.
17. Sadovnikov, S.I., Rempel, A.A. Synthesis of nanocrystalline silver sulfide. (2015) Inorg Mater 51(8): 759-766.
18. Zhu, G.X., Xu, Z. Controllable growth of semiconductor heterostructures mediated by bifunctional Ag<sub>2</sub>S nanocrystals as catalyst or source-host. (2011) J Am Chem Soc 133(1): 148-157.
19. Sadovnikov, S.I., Gusev, A.I., Rempel, A.A. Nonstoichiometry of nanocrystalline monoclinic silver sulfide. (2015) Phys Chem Chem Phys 17(19): 12466-12471.
20. Sadovnikov, S.I., Gusev, A.I., Gerasimov, E.Yu., et al. Facile synthesis of Ag<sub>2</sub>S nanoparticles functionalized by carbon-containing citrate shell. (2015) Chemical Physics Letters 642: 17-21.
21. Sadovnikov, S.I., Gusev, A.I., Rempel, A.A. An in situ high-temperature scanning electron microscopy study of acanthite-argentite phase transformation in nanocrystalline silver sulfide powder. (2015) Phys Chem Chem Phys 17(32): 20495-20501.
22. Sadovnikov, S.I., Gusev, A.I., Rempel, A.A. Nanocrystalline silver sulfide Ag<sub>2</sub>S. (2015) Reviews on Advanced Materials Science 41(1): 7-19.
23. Sadovnikov, S.I., Gusev, A.I., Chukin, A.V., et al. High-temperature X-ray diffraction and thermal expansion of nanocrystalline and coarse-crystalline acanthite  $\alpha$ -Ag<sub>2</sub>S and argentite  $\beta$ -Ag<sub>2</sub>S. (2016) Phys Chem Chem Phys 18(6): 4617-4626.
24. PANalytical B. V. PANalytical X'Pert High Score Plus. (2009) Version 2.2e (2.2.5).
25. Gusev, A.I., Rempel, A.A. Nano crystalline Materials. (2004) Cambridge Intern. Science Publ Pp: 137-150.
26. Gatan Microscopy Suite software. (2016) Gatan Inc Version 2.31.734.0.
27. <http://www.gatan.com>.
28. Horvath, B., Kawakita, J., Chikyow, T. Diffusion barrier and adhesion properties of SiO<sub>x</sub>N<sub>y</sub> and SiO<sub>x</sub> layers between Ag/polypyrrole composites and Si substrates. (2014) ACS Appl Mat Interf 6(12): 9201-9206.
29. Frueh, A.J. The crystallography of silver sulfide, Ag<sub>2</sub>S. (1958) Zeitschr Kristallographie 110(1-6): 136-144.
30. Sadanaga, R., Sueno, S. X-ray study on the  $\alpha$ - $\beta$  transition of Ag<sub>2</sub>S. (1967) Mineralogical Journal 5(2): 124-143.
31. Liu, B., Ma, Z. Synthesis of Ag<sub>2</sub>S-Ag nanoprisms and their use as DNA hybridization probes. (2011) Small 7(11): 1587-1592.
32. Terabe, K., Hasegawa, T., Nakayama, T., et al. Quantized Conductance Atomic Switch. (2005) Nature 433(7021): 47-50.
33. Kharkats, Yu.I. Electric-Field Induced Transition to Superionic Conductive State. (1981) Fiz Tverd Tela 23(7): 2190-2192.
34. Gurevich, Yu.Ya., Kharkats, Yu.I. Features of the thermodynamics of superionic conductors. (1982) Soviet Physics Uspekhi 25(4): 257-276.